

Far-Ultraviolet Observations of NGC 3516 using the Hopkins Ultraviolet Telescope

G. A. Kriss, B. R. Espey, J. H. Krolik, Z. Tsvetanov, W. Zheng, and A. F. Davidsen

Department of Physics & Astronomy, Johns Hopkins University, Baltimore, MD 21218

ABSTRACT

We observed the Seyfert 1 galaxy NGC 3516 twice during the flight of Astro-2 using the Hopkins Ultraviolet Telescope aboard the space shuttle *Endeavour* in March 1995. Simultaneous X-ray observations were performed with *ASCA*. Our far-ultraviolet spectra cover the spectral range 820–1840 Å with a resolution of 2–4 Å. No significant variations were found between the two observations. The total spectrum shows a red continuum, $f_\nu \sim \nu^{-1.89}$, with an observed flux of 2.2×10^{-14} erg cm $^{-2}$ s $^{-1}$ Å $^{-1}$ at 1450 Å, slightly above the historical mean. Intrinsic absorption in Lyman β is visible as well as absorption from O VI $\lambda\lambda 1032, 1038$, N V $\lambda\lambda 1239, 1243$, Si IV $\lambda\lambda 1394, 1403$, and C IV $\lambda\lambda 1548, 1551$. The UV absorption lines are far weaker than is usual for NGC 3516, and also lie closer to the emission line redshift rather than showing the blueshift typical of these lines when they are strong. The neutral hydrogen absorption, however, is blueshifted by 400 km s $^{-1}$ relative to the systemic velocity, and it is opaque at the Lyman limit. The sharpness of the cutoff indicates a low effective Doppler parameter, $b < 20$ km s $^{-1}$. For $b = 10$ km s $^{-1}$ the derived intrinsic column is 3.5×10^{17} cm $^{-2}$. As in NGC 4151, a single warm absorber cannot produce the strong absorption visible over the wide range of observed ionization states. Matching both the UV and X-ray absorption simultaneously requires absorbers spanning a range of 10^3 in both ionization parameter and column density.

Subject headings: galaxies: active — galaxies: individual (NGC 3516) — galaxies: nuclei — galaxies: Seyfert — ultraviolet: galaxies

1. Introduction

Only 3–10% of Seyfert 1 galaxies show intrinsic UV absorption in the resonance lines of highly ionized elements (Ulrich 1988). Of these, NGC 3516 has shown the strongest and most variable absorption lines (Ulrich & Boisson 1983; Voit, Shull, & Begelman 1987; Walter et al. 1990; Kolman et al. 1993; Koratkar et al. 1996). NGC 3516 is unusual for a Seyfert 1 in other respects as well. While as many as half of all Seyfert 1's show absorption by ionized material intrinsic to the source, characterized as a “warm absorber” (Nandra & Pounds 1994), the only Seyfert 1 besides NGC 3516 with equivalent neutral hydrogen columns exceeding 5×10^{22} cm $^{-2}$ is NGC 4151 (Kolman

et al. 1993; Nandra & Pounds 1994; Yaqoob, Warwick, & Pounds 1989; Yaqoob et al. 1993). In NGC 4151, these variable columns range from 1 to 12×10^{22} cm $^{-2}$ (Yaqoob, Warwick, & Pounds 1989; Yaqoob et al. 1993), and a similar range of variation has been observed in NGC 3516 (Kolman et al. 1993; Nandra & Pounds 1994; Kriss et al. 1996). Extended X-ray emission has been seen in the nuclei of Seyfert 2 galaxies (Wilson et al. 1992; Weaver et al. 1995), but among Seyfert 1's the only examples are NGC 4151 (Elvis, Briel, & Henry 1983; Morse et al. 1995) and possibly NGC 3516 (Morse et al. 1995). NGC 3516 is also one of the rare Seyfert 1's with an extended narrow-line region (NLR) having a biconical morphology (Ulrich & Pequignot 1980; Pogge 1989; Miyaji, Wilson, & Pérez-Fournon 1992; Golev et al. 1995). Again, NGC 4151 is the only similar counterpart (Evans et al. 1993). This rare combination of strong UV and X-ray absorption and extended narrow-line emission suggests that they may be related phenomena.

Extended narrow-line emission in Seyfert galaxies is commonly associated with photoionization by a collimated source of radiation. Biconical morphologies are most often found in Seyfert 2 galaxies (Pogge 1989; Evans et al. 1994; Schmitt & Kinney 1996), and they suggest that our line of sight to the central source of radiation is obscured. In the context of unified models of Seyfert galaxies (see the review by Antonucci 1993), Seyfert 1's present us with a direct line of sight to the broad emission-line region (BELR) and continuum source, whereas our line of sight in Seyfert 2's is blocked by a torus opaque from the mid-infrared to at least soft X-rays. If the torus collimates the ionizing radiation, then biconical morphologies should not be observed in Seyfert 1 galaxies. Given this line of reasoning, Evans et al. (1993) proposed that the UV-absorbing material on our line of sight in NGC 4151, but not in the torus proper, might collimate the ionizing radiation.

Although the strength of the UV and X-ray absorption in both NGC 4151 and NGC 3516 suggests that the two absorbing mechanisms are related, it is not clear how. Kolman et al.'s (1993) simultaneous X-ray and UV observations of NGC 3516 were inconclusive due to a lack of variability. Common UV and X-ray absorption at much weaker levels in some active galactic nuclei has been successfully modeled with a single warm absorber (Mathur et al. 1994; Mathur, Wilkes, & Elvis 1995), but the wide range of ionization states of the UV absorber in NGC 4151 is not compatible with the simplest warm absorber models (Kriss et al. 1995).

The similarities of NGC 3516 and NGC 4151 in their UV and X-ray absorption and in their biconical NLR's prompted us to explore the far-UV spectrum of NGC 3516 shortward of 1200 Å using the Hopkins Ultraviolet Telescope (HUT). Our goal was to search for further evidence that UV and X-ray absorbing gas in active galactic nuclei (AGN) is related to the collimation mechanism for the ionizing radiation. To improve our understanding of the relationship between the UV and X-ray absorbing gas, we also performed simultaneous X-ray observations using the Japanese X-ray satellite *ASCA*. In this paper we present the far-UV spectrum obtained with HUT. A companion paper (Kriss et al. 1996) discusses the *ASCA* observations.

2. Observations

We observed NGC 3516 on two occasions during the Astro-2 mission, once for 1518 s beginning at 5:35:34 UT on 1995 March 11, and again for 2200 s beginning at 1:32:03 on 1995 March 13. Both observations were through a 20" aperture during orbital night when airglow is at a minimum. The basic design of HUT is described by Davidsen et al. (1992). Briefly, a 0.9-m mirror collects light for a prime-focus, Rowland-circle spectrograph. A photon-counting detector sensitive from 820–1840 Å samples the dispersed spectrum at a resolution of 2–4 Å with ~ 0.52 Å per pixel. Improvements to HUT, its performance during the Astro-2 mission, and our basic data reduction procedures are described by Kruk et al. (1995). The raw data were reduced by subtracting dark counts, correcting for scattered geocoronal Ly α emission and subtracting airglow. We then flux-calibrated the spectrum using the time-dependent inverse sensitivity curves developed from on-orbit observations and model atmospheres of white dwarfs. Statistical errors for each pixel are calculated from the raw count spectra assuming a Poisson distribution and are propagated through the data reduction process. As there was no evidence for variability in the UV data, the two separate observations are weighted by their exposure times and combined to form the mean flux-calibrated HUT spectrum of NGC 3516 shown in Figure 1.

To model the spectrum of NGC 3516 and measure properties of the continuum, emission lines and the absorption lines, we use the IRAF¹ task **specfit** (Kriss 1994a). We fit the continuum with a power law in f_λ . The brightest broad emission lines (O VI λ 1034, Ly α , and C IV λ 1549) are well described by power law profiles while single Gaussian components are adequate for the weaker broad lines. The power law profile has a functional form $F_\lambda \propto (\lambda/\lambda_o)^{\pm\alpha}$, where $\alpha = \ln 2/(1 + \text{FWHM}/2c)$ (c.f. NGC 4151, Kriss et al. 1992). Additional narrow Gaussian cores are required for Ly α and He II λ 1640. Single Gaussian profiles are used for all absorption lines other than the Lyman series. We allow extinction to vary freely following a Cardelli, Clayton, & Mathis (1989) curve with $R_V = 3.1$.

To model hydrogen absorption in the Galaxy and in NGC 3516, we compute grids of transmission functions including transitions up to $n = 50$. Using Voigt profiles of varying column density and Doppler parameter, we then convolve the transmission with the instrument resolution. Galactic neutral hydrogen is fixed at zero redshift at a column density of 3.35×10^{20} cm $^{-2}$ (Stark et al. 1992) with a Doppler parameter of $b = 10$ km s $^{-1}$. A sharp, redshifted Lyman edge is readily apparent in the NGC 3516 spectrum. Neutral hydrogen intrinsic to NGC 3516 is permitted to vary freely in column density, redshift, and Doppler parameter.

Our best fit yields $\chi^2/\nu = 1652/1582$ for 1671 data points between 916 Å and 1800 Å (we omit a region from 1207–1222 Å surrounding geocoronal Ly α). The fitted continuum has $f_\lambda = 3.61 \times 10^{-14} (\lambda/1000\text{\AA})^{-0.11}$ erg cm $^{-2}$ s $^{-1}$ Å $^{-1}$ with $E(B - V) = 0.06 \pm 0.01$. In frequency space this corresponds to a spectral index $\alpha = 1.89$ for $f_\nu \sim \nu^{-\alpha}$. This is rather steep, but it is not

¹ The Image Reduction and Analysis Facility (IRAF) is distributed by the National Optical Astronomy Observatories, which is operated by the Association of Universities for Research in Astronomy, Inc. (AURA) under cooperative agreement with the National Science Foundation.

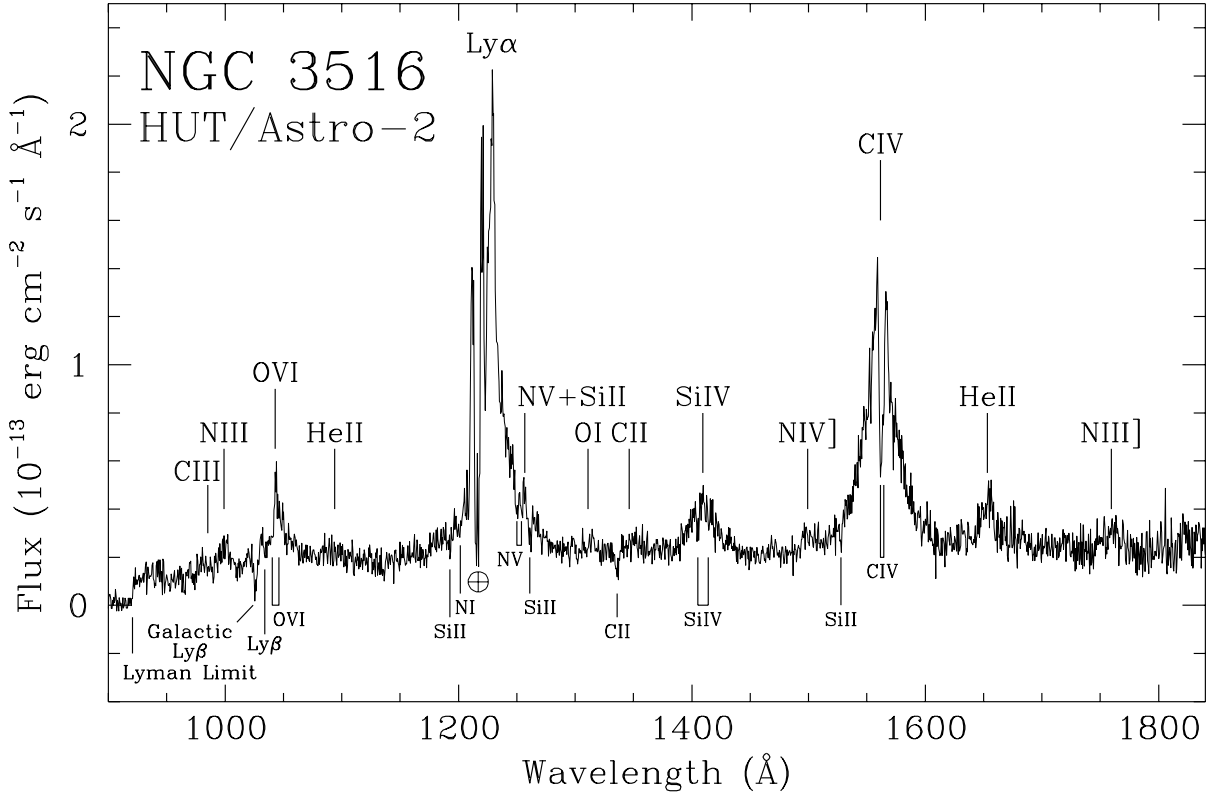


Fig. 1.— The flux-calibrated spectrum of NGC 3516 obtained with the Hopkins Ultraviolet Telescope during the Astro-2 mission is shown. Significant emission and absorption lines are marked. The indicated Lyman limit is at a redshift of 0.0075, and it is intrinsic to NGC 3516 as are the absorption lines of O VI, N V, Si IV, and C IV. The remaining absorption lines are likely galactic in origin. The earth symbol indicates the residual feature produced by subtraction of geocoronal Ly α emission.

that unusual for a low-luminosity AGN. For comparison, the Astro-1 spectrum of NGC 4151 showed a spectral index of 1.50 (Kriss et al. 1992), the FOS spectrum of NGC 1566 has $\alpha = 1.53$ (Kriss et al. 1991), and the UV continuum of M 81 has $\alpha = 1.5 - 2.0$ (Ho, Filippenko, & Sargent 1996). Our fitted extinction is higher than the predicted Galactic reddening of $E(B - V) = 0.02 - 0.03$ in the maps of Burstein & Heiles (1982), but compatible with that expected using $N_{HI} = 3.35 \times 10^{20} \text{ cm}^{-2}$ and a gas-to-dust ratio of $N_{HI}/E(B - V) = 5.2 \times 10^{21} \text{ cm}^{-2}$ (Shull & Van Steenberg 1985). Previous work based on IUE observations (Kolman et al. 1993; Koratkar et al. 1996) have determined $E(B - V) = 0.15$ based on the strength of the 2200 Å absorption feature, but such a large extinction correction provides a poor match to our data — for $E(B - V) = 0.15$, $\chi^2 = 1782$. To show the sensitivity of the data to the extinction correction, Figure 2 compares the observed spectrum with power-law continua after correction for $E(B - V) = 0.06$ and 0.15 . The figure clearly shows that no extinction correction leads to a deficit in continuum flux below 1000 Å, whereas an extinction correction of $E(B - V) = 0.15$ produces an excess in flux at short wavelengths. We suggest that

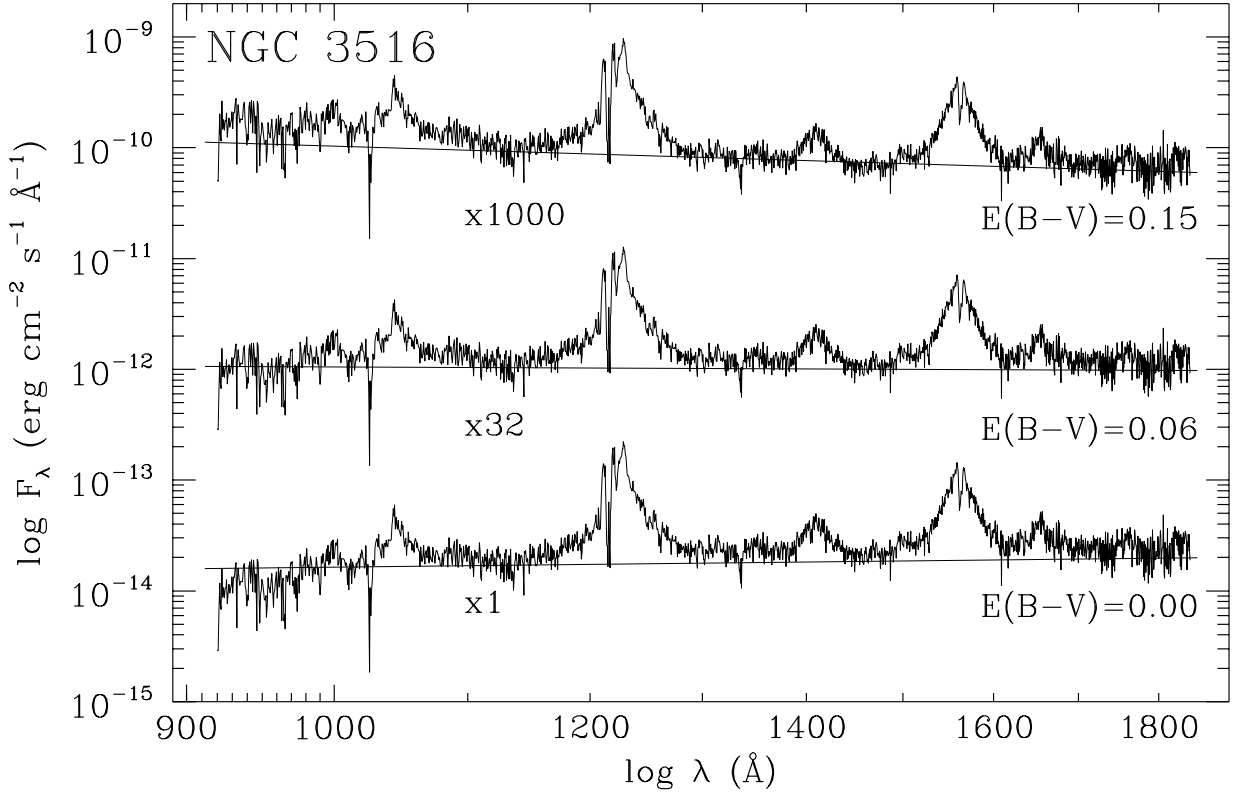


Fig. 2.— The figure shows the HUT spectrum of NGC 3516 on a log-log scale with extinction corrections applied as indicated. The spectra have been scaled up for display by the factors under each spectrum. The solid straight lines through each spectrum are the best fit power law continuum levels for the given extinction correction. No correction clearly produces a deficit in flux at short wavelengths, and $E(B - V) = 0.15$ leads to an excess in continuum flux shortward of 1000 Å. $E(B - V) = 0.06$ provides the best fit. Note that the broad wings on the emission lines leave clear continuum visible only in narrow windows shortward of 980 Å and near 1130 Å, 1450 Å and 1800 Å.

the apparent strength of the 2200 Å dip in the IUE data is not due to extinction, but rather to the onset of broad emission from blended Fe II at 2300 Å.

For the neutral hydrogen intrinsic to NGC 3516 we find a best fit redshift of $z = 0.0075 \pm 0.0005$, $N_{\text{HI}} = 3.5 \times 10^{17} \text{ cm}^{-2}$, and $b = 10 \text{ km s}^{-1}$. This is blue-shifted by $400 \pm 150 \text{ km s}^{-1}$ relative to the 2649 km s^{-1} systemic velocity of NGC 3516 measured using the stellar absorption lines (Vrtilek & Carleton 1985). The opaque Lyman limit requires neutral hydrogen with a minimum column density $N_{\text{HI}} > 2.2 \times 10^{17} \text{ cm}^{-2}$ (90% confidence). Its sharpness limits b to less than 20 km s^{-1} at 90% confidence. The effect of the assumed Doppler parameter on the shape of the intrinsic Lyman limit is shown with an enlarged view of the Lyman-limit region in NGC 3516 in Figure 3. The general weakness of the Lyman absorption lines (only Ly α and perhaps Ly β are detected) gives an upper limit of $N_{\text{HI}} < 6.3 \times 10^{17} \text{ cm}^{-2}$ at 90% confidence.

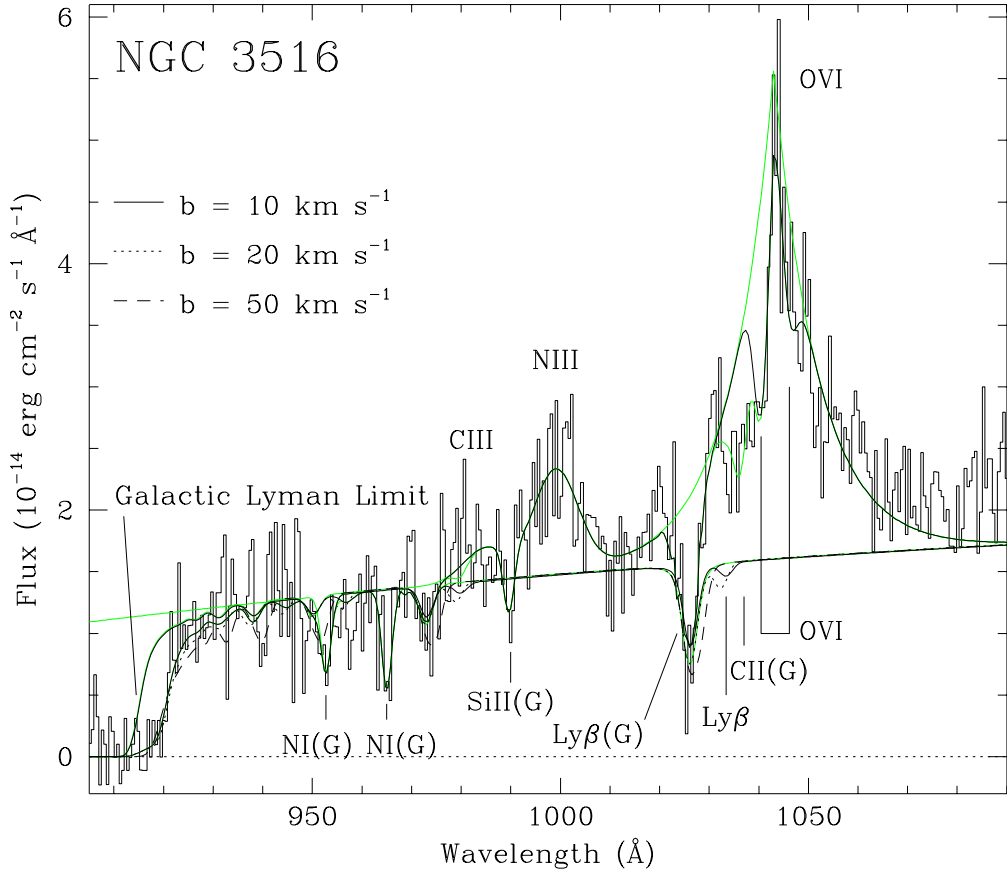


Fig. 3.— This expanded view of the short-wavelength end of the HUT spectrum shows the intrinsic Lyman limit and the O VI absorption more clearly. The position of the Galactic Lyman limit is shown to illustrate the intrinsic absorption. The solid, dotted, and dashed curves show the shape of the intrinsic Lyman absorption in NGC 3516 for assumed Doppler parameters of $b = 10, 20$, and 50 km s^{-1} , respectively. As described in the text, at 90% confidence, $b < 20 \text{ km s}^{-1}$. The heavy and light solid lines show our fit to the O VI emission and absorption. The light solid line shows the O VI emission profile superposed on the powerlaw continuum. The heavy solid line shows the contribution of the intrinsic O VI absorption to the fit. The light solid line in the vicinity of 1037 Å shows the contribution of intrinsic Ly β and Galactic C II $\lambda 1037$ to the fit. Galactic absorption features in the spectrum are denoted by a “(G)” following the line identification.

Measured properties of the fitted emission lines are in Table 1. The fitted absorption lines are summarized in Table 2. All tabulated features, except for Ly β , have a statistical significance exceeding 3σ . The error matrix of the fit is used to derive the 1σ statistical errors shown in the table. Systematic errors of up to $\sim 5\%$ are likely to be present in the fluxes, and our wavelength scale has a limiting accuracy of $\sim 60 \text{ km s}^{-1}$. For ease in fitting, some poorly constrained parameters were linked to others with better determined values. For example, the velocity offset and FWHM of the C III $\lambda 977$ and the N III $\lambda 991$ lines were linked to share common values, and the FWHM of

He II λ 1085 was set equal to that of He II λ 1640. Any entries in the tables with identical velocity offsets or FWHM's were linked in a similar manner. Since the intrinsic O VI absorption is difficult to see in Figure 1, an enlarged view illustrating our fits to this region is shown in Figure 3. The O VI absorption doublet straddles the peak of the O VI emission line, and the sharpness of the line peak is largely defined by the flux escaping at wavelengths between the doublets. Galactic C II, Galactic Ly β , and intrinsic Ly β absorption all contribute to the deficit in flux on the blue wing of the O VI emission.

Table 1. Emission Lines in the HUT Spectrum of NGC 3516

Line	λ_{vac} (Å)	Flux ^a	Velocity ^b (km s $^{-1}$)	FWHM (km s $^{-1}$)
C III	977.02	0.7 ± 0.3	-235 ± 249	3190 ± 469
N III	990.83	2.3 ± 0.3	-235 ± 249	3190 ± 469
O VI	1033.83	15.9 ± 1.1	13 ± 63	3516 ± 375
He II	1085.15	2.9 ± 0.6	-2012 ± 880	10041 ± 1694
Ly α	1215.67	5.6 ± 0.9	721 ± 33	808 ± 98
Ly α	1215.67	84.3 ± 3.1	-345 ± 160	4556 ± 230
Ly α	1215.67	89.9 ± 3.2
N V	1240.15	5.2 ± 1.0	1443 ± 339	5660 ± 181
O I	1304.35	1.3 ± 0.3	-1152 ± 573	5660 ± 181
C II	1335.30	1.9 ± 0.3	285 ± 103	5660 ± 181
Si IV	1393.76	6.1 ± 0.2	285 ± 103	5660 ± 181
Si IV	1402.77	3.1 ± 0.1	285 ± 103	5660 ± 181
N IV]	1486.50	1.1 ± 0.2	-49 ± 242	2152 ± 498
C IV	1549.05	58.4 ± 0.6	-191 ± 65	3705 ± 117
He II	1640.50	2.4 ± 0.5	-280 ± 113	1869 ± 285
He II	1640.50	5.7 ± 0.9	-280 ± 113	10041 ± 1694
He II	1640.50	8.2 ± 1.0
N III]	1750.51	2.2 ± 0.4	-1084 ± 238	2870 ± 476

^a Flux in 10^{-13} erg cm $^{-2}$ s $^{-1}$ corrected for $E(B - V) = 0.06$.

^b Velocity relative to a systemic redshift of $cz = 2649$ km s $^{-1}$ (Vrtilek & Carleton 1985).

3. The Broad Emission Lines

The broad emission lines in NGC 3516 as observed with HUT show subtle differences compared to other Seyfert 1's and low redshift AGN. The optical to X-ray spectral index for NGC 3516, $\alpha_{ox} = 1.20$, is typical of other Seyfert 1's (Kriss & Canizares 1985), but the flux ratio of O VI $\lambda 1034$ to Ly α is only 0.18. This lies below the correlation of O VI/Ly α with α_{ox} discussed by Zheng, Kriss, & Davidsen (1995), but is comparable to the mean value of 0.17 seen in high redshift quasars (Laor et al. 1994). As in the case of Fairall 9, however, the lack of a soft X-ray excess in

Table 2. Absorption Lines in the HUT Spectrum of NGC 3516

Line	λ_{vac} (Å)	EW (Å)	Velocity ^a (km s $^{-1}$)	FWHM (km s $^{-1}$)
N I	953.77	1.3 ± 0.4	-2944 ± 146	804 ± 274
N I	964.24	1.6 ± 0.5	-2392 ± 115	804 ± 274
C III	977.02	< 1.0	0	800^b
Si II	989.87	0.8 ± 0.3	-2704 ± 107	804 ± 274
Ly β	1025.72	2.1 ± 0.4	-2649 ± 156	880^b
Ly β	1025.72	0.2 ± 0.4	-400 ± 150	880^b
C II	1036.90	1.2 ± 0.3	-2798 ± 109	1076 ± 146
O VI	1031.93	1.6 ± 0.4	-161 ± 81	1076 ± 146
O VI	1037.62	0.7 ± 0.4	-161 ± 81	1076 ± 146
Si II	1193.14	2.2 ± 0.4	-2733 ± 127	1645 ± 255
N I	1200.16	2.6 ± 0.5	-2269 ± 122	1645 ± 255
Ly α	1215.67	0.5 ± 0.2	-400 ± 150	770^b
N V	1238.82	0.9 ± 0.2	63 ± 53	632 ± 116
N V	1242.80	0.4 ± 0.2	63 ± 53	632 ± 116
Si II	1260.42	1.3 ± 0.3	-2456 ± 63	831 ± 170
C II	1335.30	1.6 ± 0.3	-2454 ± 58	789 ± 146
Si IV	1393.76	0.8 ± 0.4	-204 ± 75	778 ± 585
Si IV	1402.77	0.4 ± 0.3	-204 ± 75	778 ± 585
Si II	1527.17	0.6 ± 0.2	-2495 ± 47	324 ± 106
C IV	1548.19	1.9 ± 0.1	-15 ± 22	516 ± 37
C IV	1550.77	1.0 ± 0.1	-15 ± 22	516 ± 37

^a Velocity relative to a systemic redshift of $cz = 2649$ km s $^{-1}$ (Vrtilek & Carleton 1985).

^b FWHM fixed at the instrument resolution at this wavelength.

NGC 3516 may be a significant factor in producing lower O VI/Ly α compared to other Seyfert 1's (Zheng et al. 1995).

The other noticeable difference is the relatively high strength of broad C III λ 977 and N III λ 991 emission in our spectrum. Although these lines have been seen in other low-redshift quasars (Laor et al. 1994; Laor et al. 1995), they are not detected in other HUT spectra of Seyfert 1's. The ratios of these lines to each other and to O VI λ 1034 is also typical of that seen in the low redshift quasars observed with HST (Laor et al. 1995).

Reverberation mapping experiments have shown that the broad emission-line region (BELR) of AGN is highly stratified in both spatial distribution and in ionization parameter (e.g., Clavel et al. 1991; Krolik et al. 1991; Reichert et al. 1994; Korista et al. 1995). Nevertheless, it is useful to match a single-zone photoionization model to the observed broad line emission in NGC 3516 to obtain a fiducial for comparison to other Seyferts. In addition, it provides a comparison to models of the warm absorbing medium seen in the X-ray spectrum and in the UV absorption lines that we discuss in § 4. We use the photoionization code XSTAR (Kallman & Krolik 1993) to compute a grid of photoionization models varying the total column density N and the ionization parameter $U = n_{ion}/n_H$, where n_{ion} is the number density of ionizing photons between 13.6 eV and 13.6 keV illuminating the cloud and n_H is the density of hydrogen atoms. As we are constraining only high ionization lines that are insensitive to the density, we assume constant density clouds with $n_H = 10^9$ cm $^{-3}$ and solar abundances. For the incident photoionizing continuum we use the extinction-corrected UV and absorption-corrected X-ray spectrum of NGC 3516 as described by Kriss et al. (1996). The UV power law was extrapolated to higher energies following $f_\nu \sim \nu^{-1.89}$ with a break at 51 eV to the slope of the X-ray power law, $f_\nu \sim \nu^{-0.78}$. To match the observed line ratios we varied the parameters until we achieved the closest fit to the strongest lines — O VI+Ly β , Ly α , Si IV+O IV], C IV, and He II λ 1640. The closest match is for an ionization parameter $U = 0.035$. The resulting line ratios from this model are compared to the observed values and their error bars in Table 3. Choosing $U = 0.035$ is mainly a balance between the O VI emission and the C IV line. Producing sufficient O VI requires $U = 0.045$, but then the C IV/Ly α ratio becomes too high. $U = 0.030$ fits the C IV/Ly α intensity ratio well, but the O VI emission is then a factor of 2 less than observed. As the lines we are matching originate in the high ionization illuminated faces of the BELR clouds, their intensities are rather insensitive to changes in the column density above $\log N = 21.6$ in our models.

The best-fit ionization parameter $U = 0.035$ is a typical value for single-zone models of AGN broad-line regions, but one can see from Table 3 that this model is insufficient to explain all the observed line ratios. The most noticeable differences are in the relatively high strengths observed for C III λ 977, N III λ 991, and He II λ 1640. Given the compromise we made between matching O VI and C IV, one can envision that a higher ionization zone producing relatively more O VI and He II λ 1640 could account for part of these differences. An additional population of higher density clouds may be required to produce the enhanced C III λ 977, which becomes a more important coolant as other lines become optically thick (Netzer 1990). The strong N III λ 991 is more of a

puzzle. Most photoionization models predict it to be weaker than C III λ 977, yet in our spectrum and in the HST quasar spectra (Laor et al. 1995) it is stronger. It is possible that fluorescent mechanisms could enhance the strength of this transition under favorable circumstances (Ferguson, Ferland, & Pradhan 1995).

Although the broad lines in NGC 3516 seem to be mostly produced in a region with an ionization parameter typical of the BELR in other AGN, $U = 0.035$ is an order of magnitude lower than the ionization parameter required for the warm absorbing gas detected in the ASCA X-ray spectrum (Kriss et al. 1996). This does not rule out an origin in the BELR for the X-ray warm absorbers, but these absorbers must be physically distinct from the clouds producing the bulk of the broad-line emission.

4. The Complex Absorbing Medium in NGC 3516

Intrinsic UV absorption lines are prominent in our spectrum of NGC 3516, but they are near the weakest levels seen in NGC 3516, comparable to their appearance in the 1993 IUE monitoring

Table 3. Observed and Modeled Emission Line Ratios in NGC 3516

Feature	$I/I_{\lambda 1216}^a$	Model ^b
C III λ 977	0.008 ± 0.003	0.002
N III λ 991	0.026 ± 0.004	0.000
O VI+Ly β	0.177 ± 0.014	0.123
He II λ 1085	0.032 ± 0.007	0.009
N V λ 1240	0.058 ± 0.011	0.064
O I λ 1304	0.014 ± 0.003	0.000
C II λ 1335	0.021 ± 0.003	0.007
Si IV+O IV λ 1400	0.102 ± 0.005	0.102
N IV] λ 1486	0.012 ± 0.002	0.074
C IV λ 1549	0.650 ± 0.024	0.778
He II λ 1640	0.091 ± 0.012	0.037
N III] λ 1750	0.024 ± 0.004	0.012

^a Line ratios are relative to the major contributors to the λ 1216 blend — H Ly α , He II λ 1216, and O V λ 1218.

^b Line ratio computed for a model with $U = 0.035$, $n_H = 10^9$ cm $^{-3}$, and $N = 10^{22}$ cm $^{-2}$.

campaign (Koratkar et al. 1996). The frequently observed blue-shifted absorption trough (Voit, Shull, & Begelman 1987; Walter et al. 1990; Kolman et al. 1993) is not present, and the C IV feature in our spectrum probably corresponds to the narrow component in the models of Walter et al. (1990). Although the C IV absorption line in the HUT spectrum is narrow, it is resolved. After correcting for instrumental broadening by subtracting a 2.0 Å Gaussian in quadrature (Kruk et al. 1995), we find an intrinsic width for the line of 350 km s^{-1} . This corresponds to $b = 210 \text{ km s}^{-1}$, which is consistent with the observed equivalent widths (EWs) and optically thin doublet ratio of the deblended C IV lines. The other high ionization resonance lines also have optically thin doublet ratios consistent with $b \sim 200 \text{ km s}^{-1}$. In contrast, the neutral hydrogen absorption at the Lyman limit requires $b < 20 \text{ km s}^{-1}$. This, and the significantly different velocity of the neutral hydrogen absorption, are indications that the absorbing medium contains multiple zones.

The simultaneous X-ray observations of NGC 3516 discussed in the preceding paper (Kriss et al. 1996) also hint that the absorbing medium may be complex. The ASCA observations show O VII and O VIII edges characteristic of warm absorbers that have been seen in other AGN (Turner et al. 1993; Mathur et al. 1994; Fabian et al. 1994a; Fabian et al. 1994b). Photoionized warm absorber models similar to those discussed by Krolik & Kriss (1995) can fit the data, but the fit is significantly improved if two absorbing zones with differing ionization parameter and total column density are used. These warm absorber models use the same incident photoionizing continuum described in the previous section. We also considered alternative ionizing continua to test the sensitivity of our results to the assumed incident spectrum. We used both an extremely hard spectrum with $f_\nu \sim \nu^{-0.78}$ from 2500 Å through the UV and X-ray up to 100 keV, and also the spectral shape of NGC 5548 as used by Mathur et al. (1995), which contains a soft X-ray excess. The models are computed for constant density ($n_H = 10^3 \text{ cm}^{-3}$) clouds in thermal equilibrium. (For densities $< 10^{11} \text{ cm}^{-3}$ there are no density-dependent effects in our calculations or results.) The models are described by their ionization parameter U and their total column density N .

Single-zone photoionization models of the absorbing gas in 3C 351 (Mathur et al. 1994) and in NGC 5548 (Mathur, Wilkes, & Elvis 1995) can produce both the X-ray and UV absorption seen in these two AGN. We now test whether this is true for NGC 3516. The single warm absorber fit to the ASCA spectrum of NGC 3516 has $U = 0.48$ and $\log N = 22.02$. Given the column densities predicted by this model for the UV ions, we can place the observed EWs on curves of growth (Figure 4). If the model self-consistently accounts for both the X-ray and UV absorbers, all the plotted EWs should lie on a single curve of growth. As shown in the top panel of Figure 4, they do not. The predicted column densities of neutral hydrogen and Si IV are orders of magnitude below what we observe in the HUT spectrum, and a single Doppler parameter does not give a good match to the remaining UV lines. Choosing $b = 70 \text{ km s}^{-1}$ fits the N V and O VI doublets within the errors, but this underpredicts the strength of the C IV doublet by factors of several. This situation is similar to the difficulties noted by Kriss et al. (1995) in trying to account for the low-ionization UV absorption lines in NGC 4151 with a single warm absorber model.

The warm absorber models computed with the alternative ionizing continua give similar results,

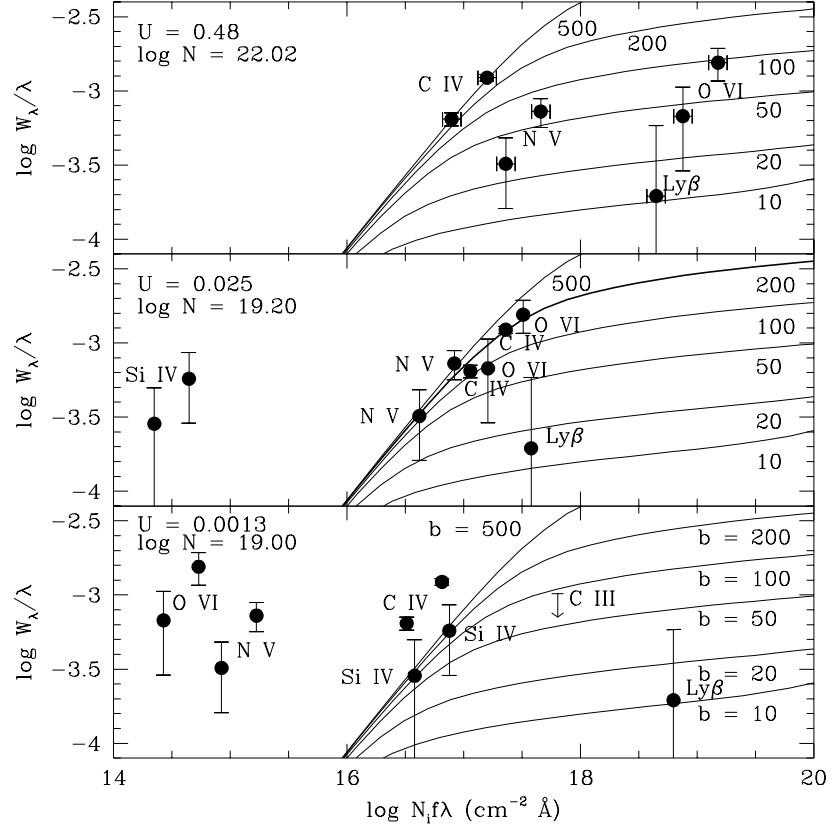


Fig. 4.— *Top Panel:* The observed EWs of the UV absorption lines in NGC 3516 are plotted on curves of growth using column densities predicted by the single warm absorber fit to the ASCA X-ray spectrum (Kriss et al. 1996). This model has $U = 0.48$ and a total column density of $10^{22.02} \text{ cm}^{-2}$. Points are plotted at a horizontal position determined by the column density for the given ion in the model with a vertical coordinate determined by the observed EW for the corresponding absorption line. The vertical error bars are from Table 2, and the horizontal error bars are the range in column density allowed by the uncertainty in the fit to the ASCA spectrum. The predicted column of Si IV in this model is too low to appear on the plot. The thin solid lines show predicted EWs as a function of column density for Voigt profiles with Doppler parameters of $b = 10, 20, 50, 100, 200$, and 500 km s^{-1} . A model that fits the data would have all points lying on one of these curves. This model cannot simultaneously match both the UV and the X-ray absorption. *Center Panel:* The observed EWs are plotted for column densities predicted by a model with $U = 0.025$ and a total column density of $10^{19.2} \text{ cm}^{-2}$. The heavy solid curve at $b = 200 \text{ km s}^{-1}$ gives a good match to the observed EWs of the C IV, N V, and O VI doublets, but the predicted EW of Si IV is far below the observed value. *Bottom Panel:* The observed EWs are plotted for column densities predicted by a model with $U = 0.0013$ and $N = 10^{19.0} \text{ cm}^{-2}$. $b = 20 \text{ km s}^{-1}$ can match the observed EWs of Si IV and Ly β and satisfy the upper limit on the EW of C III $\lambda 977$.

with the predicted columns of the UV ions in each model within tens of percent of each other. This

insensitivity to the precise shape of the ionizing spectrum is not surprising. For broad ionizing continua such as power laws or broken power laws, even the earliest photoionization calculations (e.g., Tarter, Tucker, & Salpeter 1969) showed that models were much more sensitive to ionization parameter than to spectral shape. In Table 4 we compare the columns inferred from the UV absorption lines assuming they are optically thin, as indicated by their doublet ratios, to the column densities predicted by the various models. The similarity of the models to each other is apparent, as is the large disagreement with the observations, particularly for Si IV.

The two-component warm absorber fit favored by the ASCA data also fails as an adequate description of the UV absorption. The lower ionization zone with $U = 0.32$ and $\log N = 21.84$ still falls short in matching the Si IV and H I by orders of magnitude, and once again a single Doppler parameter fails to match the observations of the remaining UV lines. The only UV-absorbing species with a significant column at any Doppler parameter in the higher ionization zone ($U = 1.66$, $\log N = 22.15$) is O VI.

Producing the observed EWs of the UV lines requires regions of lower ionization and lower column density than those producing the X-ray absorption. For $U = 0.025$, $\log N = 19.2 \text{ cm}^{-2}$, and $b = 200 \text{ km s}^{-1}$ we find a good match to the observed EWs of the C IV, N V, and O VI

Table 4. Observed and Predicted Absorption Columns in NGC 3516

Ion	N_{obs}^a (cm^{-2})	N_{Model1}^b (cm^{-2})	N_{Model2}^c (cm^{-2})	N_{Model3}^d (cm^{-2})
H I	3.5×10^{17}	5.0×10^{16}	1.7×10^{17}	1.8×10^{16}
C IV	4.7×10^{14}	4.7×10^{14}	6.0×10^{14}	5.4×10^{14}
N V	4.1×10^{14}	2.1×10^{15}	2.5×10^{15}	3.2×10^{15}
O VI	1.3×10^{15}	9.8×10^{16}	1.1×10^{17}	1.4×10^{17}
Si IV	1.1×10^{14}	$< 1 \times 10^{10}$	$< 1 \times 10^{10}$	$< 1 \times 10^{10}$

^aColumn density assuming the observed absorption lines are optically thin. The H I column is from the Lyman-limit fit.

^bPredicted column density for the single-zone warm absorber model with the NGC 3516 ionizing spectrum, $U = 0.48$ and $\log N = 22.02$.

^cPredicted column density for the warm absorber model with the $\nu^{-0.78}$ ionizing spectrum, $U = 0.16$ and $\log N = 22.02$.

^dPredicted column density for the warm absorber model with the NGC 5548 ionizing spectrum, $U = 1.47$ and $\log N = 22.02$.

doublets as shown in the center panel of Figure 4. The predicted EW of the Ly β line is $\sim 2\sigma$ higher than observed, but enhancing the overall metal abundance by a factor of a few can correct this. However, the predicted EW of Si IV in this model is orders of magnitude below the observed value. Similar problems are encountered in matching the inferred column densities of Si IV absorption in models of broad-absorption line (BAL) QSOs (Weymann, Turnshek, & Christiansen 1985). *Ad hoc* adjustments to the ionizing continuum can alleviate the disagreement to some extent (Weymann, Turnshek, & Christiansen 1985), but even the most extreme changes do not bring the predictions within the bounds of the observations, again showing the relative insensitivity of photoionization models to the shape of the ionizing spectrum. Producing enough Si IV absorption requires a zone of even lower ionization. Choosing $U = 0.0013$ and $\log N = 19.0$ matches the Si IV EWs without contributing much to the columns of the higher ionization lines. This model is illustrated in the lower panel of Figure 4. Limits on the EWs of lower ionization species such as Ly β and C III $\lambda 977$, however, require $b < 50 \text{ km s}^{-1}$. This lower ionization zone with low Doppler parameter is potentially the origin of the optically thick Lyman limit system, but the predicted column of neutral hydrogen in this model is only $N_{HI} = 7.7 \times 10^{16} \text{ cm}^{-2}$, a factor of 4 below the observed value.

The multiple zones considered above span a range of 10^3 in both column density and ionization parameter, and they form a nearly orthogonal set that makes it possible to consistently model the UV and X-ray absorption with separate regions of gas in very different physical states. For Doppler parameters at the sound speed of the two high ionization zones producing the X-ray absorption (30 km s^{-1} in the lower ionization zone, 70 km s^{-1} in the higher), the predicted contribution of the X-ray absorbing gas to the EWs of the C IV, N V, and O VI lines is only 20–30% of their observed values. The UV zones producing the C IV, N V, O VI and Si IV lines have total columns with negligible impact on the X-ray opacity. Since the X-ray absorbing gas is predicted to have a significantly lower Doppler parameter than the gas producing the bulk of the UV absorption lines, high resolution spectra in the UV should be able to identify kinematic components associated with the different zones.

Several previous authors have suggested that the UV absorption lines and the X-ray absorption seen in some AGN may have a common origin in BELR clouds (Ferland & Mushotzky 1982; Reichenert, Mushotzky, & Holt 1986). However, Mathur et al. (1994) show that the physical conditions of the UV and X-ray absorber in 3C 351 are different from those of the BELR clouds, with the X-ray warm absorber requiring a much higher ionization parameter than the clouds producing the broad emission lines. For NGC 3516, Voit, Shull, & Begelman (1987) argued that the observed absorption profile (the C IV absorption in the 1980's was much broader and stronger than observed here) required 10–30 BELR clouds along the line of sight and that photoionized C IV could not be present in the outer clouds due to shielding by the inner ones. The lack of observed Mg II absorption was another difficulty for models involving BELR clouds. They concluded that the absorption must arise in optically thin, outflowing material with a density exceeding 10^5 cm^{-3} , given the observed variability, and that it could not be associated with typical BELR clouds.

Our conclusions are similar, even though the absorption is now much weaker. The ionization parameter we derive for the broad emission-line clouds ($U \sim 0.035$) is an order of magnitude lower than that required by the X-ray absorbing gas, making it highly unlikely that the X-ray absorption occurs in BELR clouds. $U \sim 0.035$, however, is similar to the ionization parameter we find for the zone producing the C IV, N V, and O VI absorption lines ($U \sim 0.025$). Although these absorption lines and the broad emission lines share comparable ionization parameters, the total columns of the BELR clouds are $\sim 10^3 \times$ higher, as the broad emission line clouds are optically thick in these transitions, but the absorbing clouds are optically thin. This column density constraint is a poor one, however, because the BELR is highly stratified, and there may well be a population of clouds that both make the absorption lines and contribute to the broad-line emission. The velocity distribution of such clouds would have to be rather peculiar, however, to project a velocity width of only 200 km s^{-1} along the line of sight from an ensemble with an emission line width of $\sim 4000 \text{ km s}^{-1}$. We conclude that we still cannot unambiguously establish the location of the absorbing gas, but it must be physically distinct from the broad emission line clouds.

Although we have described the UV and X-ray absorbing zones as discrete entities, it is quite likely that there is a broad, possibly continuous, distribution of parameters such as one might find in an outflowing wind, either from the accretion disk or from the surface of the obscuring torus. As discussed in the introduction, NGC 3516 is one of the rare Seyfert 1 galaxies that shows an extended, biconical NLR (see Golev et al. 1995 for the best images). Among Seyfert 1's, only NGC 4151 has such an extensive NLR with a biconical morphology (Pogge 1989; Evans et al. 1994; Schmitt & Kinney 1996). The biconical morphology in NGC 3516 implies that our line of sight passes close to the surface of the obscuring torus as suggested for NGC 4151 by Evans et al. (1993). The opaque Lyman limit is another characteristic that NGC 3516 shares with NGC 4151. These features are unusual in combination for a Seyfert 1, and their presence in yet another galaxy strengthens the case for collimation of the ionizing radiation by the absorbing gas.

The complexity of the UV and X-ray absorption that both NGC 3516 and NGC 4151 exhibit suggest that the inclination of the source relative to the observer may lead to the differences between these two objects and the apparently simpler cases considered by Mathur et al. (1994,1995). The simpler warm absorbers with only high-ionization UV absorption lines may be viewed at higher inclination, further away from the denser medium near the torus. Such geometrical differences may ultimately help us to understand the location and origin of the warm absorbing gas in AGN.

This work was supported by NASA contract NAS 5-27000 to the Johns Hopkins University.

REFERENCES

Antonucci, R. R. J. 1993, *ARA&A*, 31, 473

Burstein, D., & Heiles, C. 1982, *AJ*, 87, 1165

Cardelli, J., Clayton, G., & Mathis, J. 1989, *ApJ*, 345, 245

Clavel, J., et al. 1991, *ApJ*, 366, 64

Davidsen, A. F., et al. 1992, *ApJ*, 392, 264

Elvis, M., Briel, U. G., & Henry, J. P. 1983, *ApJ*, 268, 105

Evans, I. N., Ford, H. C., Kriss, G. A., & Tsvetanov, Z. 1994, in *The First Stromlo Symposium: The Physics of Active Galaxies*, ASP Conf. Ser. 54, ed. G. V. Bicknell, M. A. Dopita, & P. J. Quinn, (San Francisco: ASP), p. 3

Evans, I., Tsvetanov, Z., Kriss, G. A., Ford, H. C., Caganoff, S., & Koratkar, A. P. 1993, *ApJ*, 417, 82

Fabian, A., Nandra, K., Brandt, W., Hayashida, K., Makino, F., & Yamauchi, M. 1994, in *New Horizons in X-ray Astronomy*, eds. F. Makino & T. Ohashi (Tokyo: Universal Academy Press), p. 573

Fabian, A., et al. 1994, *PASJ*, 46, L59

Ferguson, J. W., Ferland, G. J., & Pradhan, A. K. 1995, *ApJ*, 438, L55

Ferland, G. J., & Mushotzky, R. F. 1982, *ApJ*, 262, 564

Golev, V., Yankula, I., Bonev, T., & Jockers, K. 1995, *MNRAS*, 273, 129

Halpern, J. 1984, *ApJ*, 281, 90

Ho, L., Filippenko, A., & Sargent, W. L. W. 1996, *ApJ*, in press

Holt, S. S., et al. 1980, *ApJ*, 241, L13

Kallman, G. A., & Krolik, J. H. 1993, NASA Internal Report

Kolman, M., Halpern, J. P., Martin, C., Awaki, H., & Koyama, K. 1993, *ApJ*, 403, 592

Koratkar, A., et al. 1996, in preparation

Korista, K., et al. 1995, *ApJS*, 97, 285

Kriss, G. A. 1994a, in *Astronomical Data Analysis Software and Systems III*, ASP Conf. Ser. 61, ed. D. R. Crabtree, R. J. Hanisch, & J. Barnes, (San Francisco: ASP), 437

Kriss, G. A., & Canizares, C. R. 1985, *ApJ*, 297, 177

Kriss, G. A., Davidsen, A. F., Zheng, W., Kruk, J. W., & Espey, B. R. 1995, *ApJ*, 454, L7

Kriss, G. A., et al. 1991, *ApJ*, 377, L13

Kriss, G. A., et al. 1992, *ApJ*, 392, 485

Kriss, G. A., et al. 1996, *ApJ*, this issue

Kriss, G. A., Tsvetanov, Z., & Davidsen, A. F. 1994b, in *The First Stromlo Symposium: The Physics of Active Galaxies*, ASP Conf. Ser. 54, ed. G. V. Bicknell, M. A. Dopita, & P. J. Quinn, (San Francisco: ASP), p. 281

Krolik, J.H., Horne, K., Kallman, T.R., Malkan, M.A., Edelson, R.A., & Kriss, G.A. 1991, *ApJ*, 371, 541

Krolik, J. H., & Kriss, G. A. 1995, *ApJ*, 447, 512

Kruk, J. W., Durrance, S. T., Kriss, G. A., Davidsen, A. F., Blair, W. P., Espey, B. R., & Finley, D. 1995, *ApJ*, 454, L1

Laor, A., Bahcall, J. N., Jannuzi, B. T., Schneider, D. P., Green, R. F., & Hartig, G. F. 1994, *ApJ*, 420, 110

Laor, A., Bahcall, J. N., Jannuzi, B. T., Schneider, D. P., Green, R. F., & Hartig, G. F. 1995, *ApJS*, 99, 1

Mathur, S., Wilkes, B., Elvis, M., & Fiore, F. 1994, *ApJ*, 434, 493

Mathur, S., Wilkes, B., & Elvis, M. 1995, *ApJ*, 452, 230

Miyaji, T., Wilson, A. S., & Pérez-Fournon, I. 1992, *ApJ*, 385, 137

Morse, J., Wilson, A. S., Elvis, M., & Weaver, K. A. 1995, *ApJ*, 439, 121

Nandra, P., & Pounds, K. A. 1994, *MNRAS*, 268, 405

Netzer, H. 1990, in *Active Galactic Nuclei*, ed. T. J. L. Courvoisier & M. Mayor (Berlin: Springer), p. 57

Netzer, H. 1993, *ApJ*, 411, 594

Pogge, R. 1989, *ApJ*, 345, 730

Reichert, G. A., et al. 1994, *ApJ*, 435, 582

Reichert, G. A., Mushotzky, R. F., & Holt, S. S. 1986, *ApJ*, 303, 87

Schmitt, H. R., & Kinney, A. L. 1996, *ApJ*, in press

Shull, J. M., & Sachs, E. R. 1993, *ApJ*, 416, 536

Shull, J. M., & Van Steenberg, M. E. 1985, *ApJ*, 294, 599

Stark, A.A., et al. 1992, *ApJS*, 79, 77

Tarter, C. B., Tucker, W. H., & Salpeter, E. E. 1969, *ApJ*, 156, 943

Turner, T.J., Nandra, K., George, I.M., Fabian, A.C., & Pounds, K.A. 1993, *ApJ*, 419, 127

Ulrich, M.-H. 1988, *MNRAS*, 230, 121

Ulrich, M.-H., & Boisson, C. 1983, *ApJ*, 267, 515

Ulrich, M.-H., & Pequignot, D. 1980, *ApJ*, 238, 45

Voit, G. M., Shull, J. M., & Begelman, M. C. 1985, *ApJ*, 316, 573

Vrtilek, J. M., & Carleton, N. A. 1985, *ApJ*, 294, 106

Walter, R., Ulrich, M.-H., Courvoisier, T. J.-L., & Buson, L. M. 1990, *A&A*, 233, 53

Weaver, K. A., Mushotzky, R. F., Serlemitsos, P. J., Wilson, A. S., Elvis, M., & Briel, U. 1995, *ApJ*, 442, 597

Wilson, A. S., Elvis, M., Lawrence, A., & Bland-Hawthorne, J. 1992, *ApJ*, 391, L75

Weymann, R. J., Turnshek, D. A., & Christiansen, W. A. 1985, in *Astrophysics of Active Galaxies and Quasi-stellar Objects*, ed. J. S. Miller (Mill Valley: University Science Books), 333

Yaqoob, T., Warwick, R. S., & Pounds, K. A. 1989, *MNRAS*, 236, 153

Yaqoob, T., et al. 1993, *MNRAS*, 262, 435

Zheng, W., Kriss, G. A., & Davidsen, A. F. 1995, *ApJ*, 440, 606

Zheng, W., Kriss, G. A., Davidsen, A. F., & Kruk, J. W. 1995, *ApJ*, 454, L11